 doi:10.20944/preprints201810.0164.v1

Article

Spatio-temporal Variation Analysis of Landscape Pattern Respond to Land Use Change from 1985 to 2015 in Xuzhou City, China

Yantao Xi[1, 2,*], Nguyen Xuan Thinh[2], Cheng Li[2]

[1] School of Resources and Geosciences, China University of Mining and Technology, Xuzhou 221116, China; xyt556@cumt.edu.cn
[2] School of Spatial Planning, TU Dortmund, Dortmund 44227, Germany; nguyen.thinh@tu-dortmund.de
[*] Correspondence: xyt556@cumt.edu.cn; Tel.: +86-516-8359-0106

Abstract: Rapid urbanization has dramatically spurred the economic development over the past three decades, especially in China, but has nevertheless had negative impacts on natural resources since it is an irreversible process. Thus, it is essential to timely monitor and quantitatively analysis the changes in land use over time and to identify the landscape pattern variation related to growth mode in different period. This study aims at inspecting spatiotemporal characteristics of landscape pattern respond to land use changes in Xuzhou city during the period from 1985 to 2015. In this connection, we proposed a new spectral index, named the Normalized Difference Enhanced Urban Index (NDEUI), which combines data from NTL (Nighttime light) from the Defense Meteorological Satellite Program/Operational Linescan System (DMSP/OLS) with annual maximum Enhanced Vegetation Index (EVI) to reduce the detection confusion between urban areas and barren land, as well as follows. NDEUI-assisted Random Forests algorithm was implemented to obtain the land use/land cover (LULC) maps of Xuzhou in 1985, 1995, 2005 and 2015, respectively. Here, four different periods viz. 1985–1995, 1995–2005, 2005-2015 and 1985–2015 are chosen for the change analysis of land use and landscape pattern. The results indicated that the urban area has increased by about 30.65%, 10.54%, 68.77%, and 143.75% during the four periods mentioned above at the main expense of agricultural land, respectively. The spatial trend maps revealed that continuous transition from other land use types into urban land has appeared a dual-core development mode throughout the urbanization process, located at the new city region and the Jiawang district, mainly affected by the construction of new city region, freeway and the high railway station. Furthermore, we quantified the patch complexity, aggregation, connectivity and diversity of landscape employing a number of landscape metrics to represent the changes of landscape pattern at both class and landscape level, affected by urbanization during the study period. The results showed that with regard to the four aspects of landscape pattern, there were considerable differences among the four years, mainly owing to the increasing dominance of urbanized land. Spatiotemporal variation of landscape pattern was also conducted on the basis of subgrids in 900m×900m. Combined with the land use changes and spatiotemporal variation of landscape pattern, it can be concluded that different urbanization modes and intensity result in variously the spatiotemporal evolution of landscape patterns. For Xuzhou city, the urban growth mainly appeared a leapfrog mode alone both sides of the roads during the period of 1985 to 1995, and then shifted into edge-expansion mode during the period from 1995 to 2005, whereas the edge-expansion and leapfrog modes coexisted for the period from 2005 to 2015. The high valuable spatiotemporal information generated utilizing RS and GIS in this study may give assistance to urban planners and policymakers to well understand urban dynamics and evaluate their spatiotemporal and environmental impacts at a local level for the sake of sustainable urban planning in the future.

Keywords: Land use/land cover; Nighttime light (NTL); NDEUI, Landscape metrics; Random Forests; Urban growth mode

1. Introduction

In China, significant economic development has resulted in rapid expansion of the urban area of city during the past three decades creating tremendous stresses on the environment, natural resources, and public health [1-4]. Dynamic change monitoring and quantifying of urban areas play a critical role in studying urban growth modeling [5, 6], urban heat islands [7, 8], and land cover changes [9-11]. Accurately and long-termly monitoring on urban dynamics is essential for understanding the consequences of urbanization and subsequently to regulate it at regular intervals [2]. Therefore, urban expansion has increasingly become a major issue facing many fast developing cities with the rapid growth of the urban population and intensive human activities [5, 12].

Remote sensing provides us a useful tool to monitor and quantify land use/land cover (LUCC) change at high spatial resolution and annual temporal scales, so as to systematically track the magnitude and trends of urbanization[2, 5, 13]. Several LULC datasets have been developed using remote sensing, such as the 500-m Moderate-Resolution Imaging Spectroradiometer Global Yearly Land Cover Type (MCD12Q1, from 2001 to 2013) [14], 30-m National Land Cover Database (NLCD, 1992, 2001, 2006, 2011) [15], and the 30-m Finer Resolution Observation and Monitoring-Global Land Cover (GLOBELAND30, 2000,2010) [16]. However, they are either not accurate enough for city-level research or lack in sufficient temporal resolution, and are not useful in characterizing the urban long-term spatial-temporal dynamics [17-19]. Thus, various approaches have been proposed to derive urban land from different remote sensing images, such as spectral mixture analysis [20, 21], object-based approach [22, 23], multivariate texture approach [1]. In addition, due to the optical spectral complexity of urban land and confusion with bare lands and fallow land, it is extremely difficult to accurately extract urban land using a single sensor with a limited spectral range[24]. Various indices were also involved in enhancing urban lands to make them more distinguishable from other lands, such as the multi-source Normalized Difference Impervious Surface Index (MNDISI) [25], the Biophysical Composition Index (BCI) [26], the Enhanced Built-Up and Bareness Index (EBBI) [27], Normalized Difference Urban Index (NDUI) [28], Normalized Difference Bareness Index (NDBaI) [29]. For instance, MNDISI combines Landsat surface temperature and fine resolution International Space Station night light images to highlight urban areas. However, temperature can vary significantly with terrain changes. Furthermore, finer resolution night light images are not available for the entire globe and for multiple times.

To track multi-temporal trajectory of urban, change detection techniques have been widely employed for comparison of paired images. Image differencing, principal component analysis and post-classification comparison are the most common methods [30]. Note that no single approach is optimal and applicable to all cases [31]. The Landsat series data (Thematic Mapper, TM; Enhanced Thematic Mapper plus, ETM+; and Operational Land Imager, OLI) are useful for change detection due to their high temporal-spatial resolution, spectral resolution [32]. Reynolds, Liang, Li and Dennis [2] present a temporal trajectory polishing method to generate high frequency, high accuracy, and consistent trajectories of urban land-cover change in NWA. Son, et al. [33] explored the urban growth using the linear mixture model in HCMC through Landsat images. Villa [34] proposed the Soil and Vegetation Index (SVI) and utilized the multi-temporal SVI ratios thresholding for identifying urban growth area.

Understanding the dynamic change of landscape patterns is critical to revealing the process of urbanization and its impacts on the environment [12, 35, 36]. Landscape metrics have been widely used to quantify landscape patterns and analyze the dynamic changes of the regional landscape [37]. Liu and

Yang [38] utilized landscape metrics to characterize land use changes and reveal the underlying processes of urban sprawl. Due to the spatial heterogeneity, landscape patterns changes can be used to indicate the spatial distribution of urbanization modes. [35]. On the basis of the spatial variation analysis of landscape pattern and its related built-up growth, Yang, Wong, Chen and Chen [12] evaluated and modeled the relationship between the urban sprawl characters and landscape pattern based on different temporal scales.

In this study, we attempt to highlight urban areas by integrating the medium resolution Landsat and the coarse resolution DMSP/OLS nighttime light (NTL) data considering both of them with long historical archives. There are two key issues. Firstly, we derive the maximum Enhanced Vegetation Index (EVI) of each pixel from the Landsat 32-Day EVI Composites and generate the "Max EVI" composite annually. It is helpful to maximize the separability between fallow lands and urban areas. Secondly, we construct and calculate a normalized difference NTL-EVI index (NDNEI) combining "Max EVI" composite with normalized NTL data, which is effective to distinguish between the urban area and bare land or rural settlements. Then, the Random Forest (RF) was employed as a basic classifier to obtain annual classification result based on the original spectral bands, as well as NDNEI. All the above are implemented on a cloud computing platform, which is the Google Earth Engine (GEE). This study aimed to monitor and reveal land use change and urban spatial expansion patterns in the Xuzhou city during the past three decades. Furthermore, landscape pattern would be analyzed at the metric levels of class and landscape to understand the process of urbanization and its impacts on the environment. To understand the process of urbanization and its impacts on the environment, it is critical to developing a systematic approach that includes both spatiotemporal monitoring and landscape pattern analysis. Finally, we quantify the LULC changes, landscape pattern and analysis trends of urban sprawl in Xuzhou from 1985 to 2015.

2. Material and Methodology

2.1 Study Area

Xuzhou (33º43'-34º58'N, 116º22'-118º40'E) is located in the northwest of Jiangsu Province, China, adjacent to Shandong, Henan, and Anhui provinces (Figure 1). There is about 300km away from Xuzhou to Nanjing, Jinan, Zhengzhou and Hefei, the capitals of adjacent provinces. It is also the center city of Huaihai Economic Zone, with the area of 17.6 million km^2 and the population of 120 million. Xuzhou is the largest city among the adjacent 19 cities, consisting of 5 administrative districts, 3 counties and 2 county-level cities. It is mostly comprised of plains, with small areas of hillocks and mountains in the central and eastern regions. The Old Yellow River flows across the city generally in the west to southeast direction, and the Yunlong Lake locates in the south of the region. For the purpose of this study, the central area of the city was selected, which is composed of four districts, namely Quanshsn, Gulou, Yunlong and Jiawang district. It covers an area of 1058 km^2. During the three past decades, Xuzhou has experienced significant economic growth and rapid urbanization. The urban population increased from 0.67 million in 1978 to approximately 2.02 million in 2015. The GDP has raised to 531.952 billion RMB Yuan in 2015 against 2.14 billion in 1978 (Figure 2).

Preprints (www.preprints.org) | NOT PEER-REVIEWED | Posted: 9 October 2018 doi:10.20944/preprints201810.0164.v1

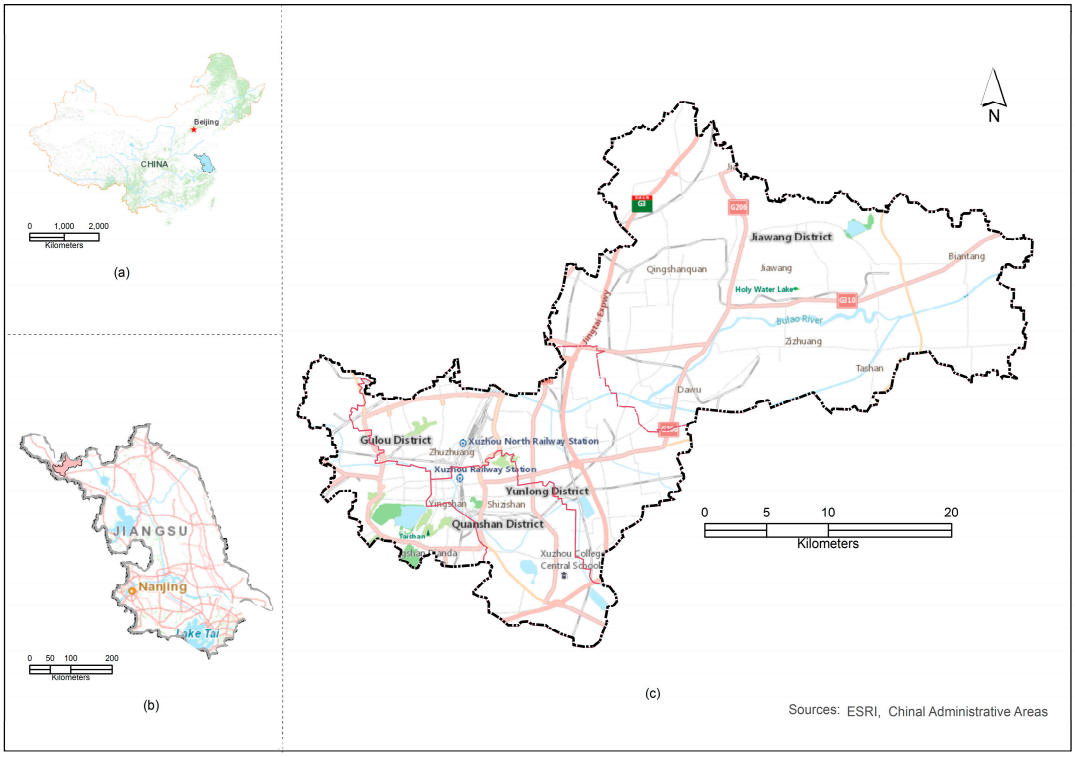

Figure 1. Map of China showing the location of Jiangsu province (Data Source: ESRI); (b) Map of Jiangsu province showing the location of Xuzhou city center (Data Source: ESRI); and (c) Map of study area

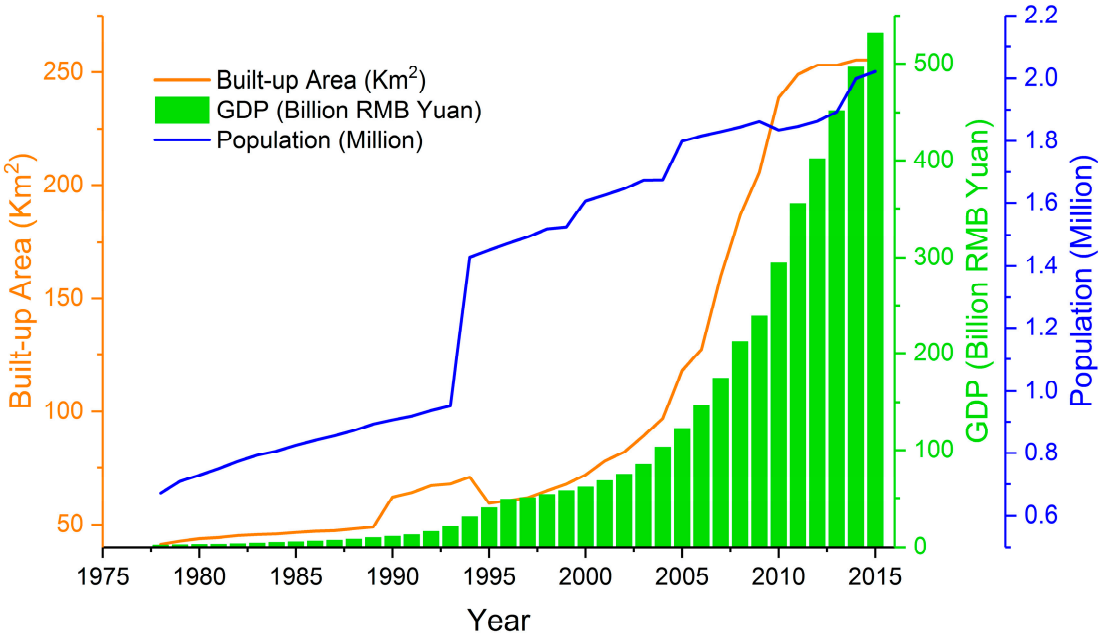

Note: In 1993 and 2000, some administrative divisions were adjusted.

Figure 2. Population, built-up area and GDP growth of Xuzhou from 1978 to 2014 (Data Source: Statistical Yearbook of Xuzhou City)

Preprints (www.preprints.org) | NOT PEER-REVIEWED | Posted: 9 October 2018 doi:10.20944/preprints201810.0164.v1

135 *2.2 Data and Preprocessing*

136 The analysis of land use changes and landscape pattern were conducted on the basis of post-
137 classification change detection strategy. The procedural workflow proposed in this study is illustrated in
138 Figure 3. Each component will be described in detail as follows, including data sources and pre-
139 processing, classification scheme, land use change and landscape pattern analysis.

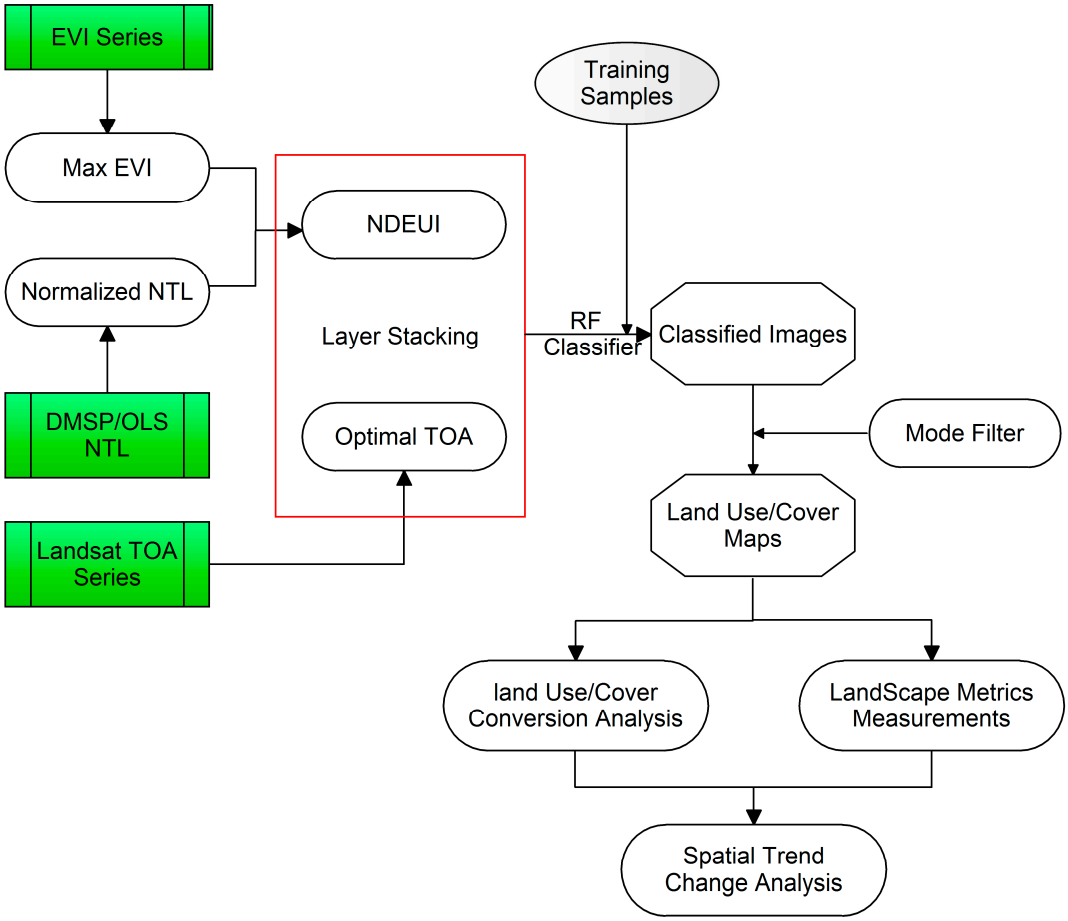

140

141 Figure 3. Flowchart of the procedural workflow.

142 2.2.1 Landsat time series

143 With the free access to Landsat archive and other new remote sensing data sources online, it is
144 possible to exploit the multi-temporal remote sensing data to map urban changes. Google Earth Engine
145 is a cloud-based platform for planetary-scale environmental data analysis. It combines a petabyte-scale
146 archive of publicly available remotely sensed imagery and other data. Landsat series TOA Reflectance
147 data (Orthorectified) are involved in this study, including Landsat TM, ETM+ and Landsat OLI. They are
148 made from Level L1T orthorectified scenes, using the computed Top-of-Atmosphere (TOA) reflectance
149 [39]. These composites are created from all the scenes in each 32-day period beginning from the first day
150 of the year and continuing to the 352nd day of the year. The last composite of the year, beginning on day
151 353, will overlap the first composite of the following year by 20 days. All the images from each 32-day
152 period are included in the composite, with the most recent pixel as the composite value.
153 To avoid the confusion between new urban land and other land cover types (such as bare land,
154 follow or post-harvest cropland), it can be resolved combining images from multiple seasons (Figure 4).

Preprints (www.preprints.org) | NOT PEER-REVIEWED | Posted: 9 October 2018 doi:10.20944/preprints201810.0164.v1

There is often a high probability that bare or cropland will be vegetated during at least one season of each year, and thus can be separated from built-up areas predominantly non-vegetated all the year round. However, it is unrealistic to select all the seasonal imageries in a year.

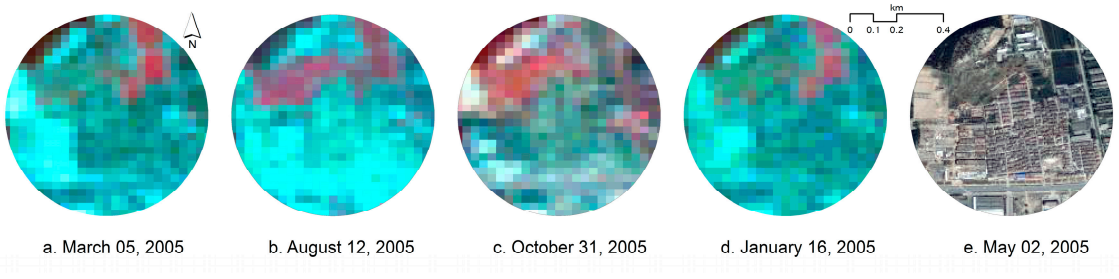

Figure 4. Multispectral seasonal observations of built-up land and cropland from 30-m resolution Landsat TM data in 2005 in a peri-urban area northwest of Xuzhou (the Near-infrared, Red and Green wavelengths are set to R-G-B, a reference of the same area is shown in (e) from Google Earth).

Apart from the raw data or preprocessing data, Google Earth Engine also provide all kinds of Composite product derived from raw data, such as 32-Day Composite for NDWI, NDVI, EVI. In this study, we compared 32-Day NDVI Composite with the EVI Composite (Figure 5). For EVI, it is clear that all the land use types have better separability, especially in summer (Figure 5). For Crop/Grass land, the EVI has a high value than corresponding NDVI, the max value up to 1. Thus, the EVI was employed in this study, which is generated from the Near-IR, Red and Blue bands of each scene, and ranges in value from -1.0 to 1.0 [40] (Eq.(1)).

$$EVI = 2.5 \times \frac{\rho_{NIR} - \rho_{Red}}{\rho_{NIR} + 6 \times \rho_{Red} - 7.5 \times \rho_{Blue} + 1} \quad (1)$$

Where ρ_{Blue}, ρ_{Red} and ρ_{NIR} are the top-of-atmosphere (TOA) reflectance of Blue, Red and NIR bands for Landsat series imagery.

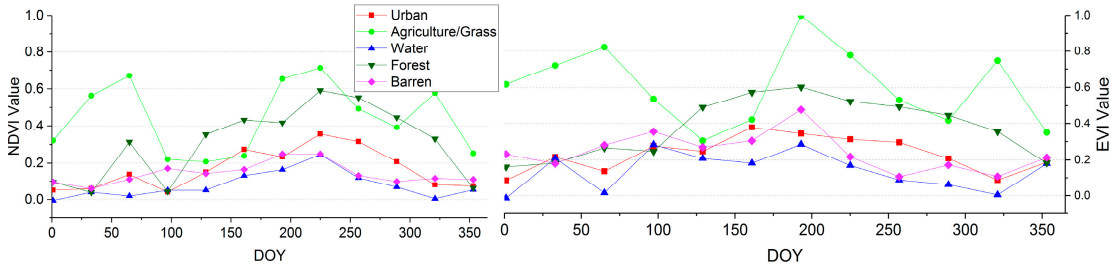

Figure 5. Comparison between the NDVI and EVI, derived from the Landsat 8 32-Day NDVI Composite and EVI Composite in 2016

2.2.2 DMSP/OLS NTL data

The version 4 DMSP/OLS NTL data from the website of the National Geophysical Data Center at the National Oceanic and Atmospheric Administration were also hosted on Google Earth Engine, which is aggregated and composited to 30 arc second (about 1 km) grids (https://ngdc.noaa.gov/eog/dmsp/downloadV4composites.html). It has a unique capability to detect visible and near-infrared (VNIR) emission sources at night. Each image in the collection contains 4 bands, i.e. avg_vis, cf_cvg, avg_lights_x_pct and stable_lights. The cleaned up avg_vis (stable_lights) was selected in our study, which contains the lights from cities, towns, and other sites with persistent lighting, including gas flares. Ephemeral events, such as fires have been discarded. The background noise was identified and replaced with values of zero. The DN values of this band range from 0 to 63.

Preprints (www.preprints.org) | NOT PEER-REVIEWED | Posted: 9 October 2018 doi:10.20944/preprints201810.0164.v1

185 2.2.3 Data pre-processing

186 32-Day EVI Composites precede the NDVI Composites in distinguishing among the different land
187 use (Figure 5). Thus, 32-Day EVI Composites were involved in this study. Due to growth cycle and
188 seasonality of crop, it is difficult to determine the optimal TOA reflectance data for each year, which is
189 also affected by the clouds. Thus, in order to overcome the limitations, one effective approach is to
190 produce a maximum EVI image from multi-temporal EVI images. In this study, 32-Day EVI Composites
191 were selected for each year, which consist of 12 EVI images. For each pixel, we got the maximum of EVI
192 over the year and generated the EVI_{max} imagery for each year. Another important role for the EVI_{max}
193 imagery is to remove the impact of cloud contamination. Therefore, the final EVI_{max} imagery is cloud-free
194 and has a data range between -1 and 1.
195 Due to the lack of on-board calibration and the difference between sensors, there are systematic
196 biases in NTL data. Consequently, the NTL data the individual composites had to be inter-calibrated
197 carefully to generate a consistent NTL time series [41-43]. Elvidge, Hsu, Baugh and Ghosh [43] . Pandey,
198 et al. [44] compared and evaluated existing nine calibration methods to provide guidance to us on their
199 relative strengths and weaknesses. This research results showed that inter-calibration reduces systematic
200 biases consistently across most countries using the methods adopted in [43] and [45]. Pandey, Zhang and
201 Seto [44], and suggests that Zhang, Pandey and Seto [45] can obtain marginally better results than
202 Elvidge, Hsu, Baugh and Ghosh [43].The coefficients for inter-calibration provided by Zhang, Pandey
203 and Seto [45] were adopted in our study.
204 While the calibrated DMSP/OLS NTL values are not recorded in the range [-1, 1], EVI values are
205 generated in the range [−1.0, 1.0]. To make them comparable, we normalize the calibrated DMSP/OLS
206 NTL into the range of [0.0, 1.0]. Then, we resample the normalized DMSP/OLS NTL data down to 30 m.

207 2.2.4 The Normalized Difference Enhanced Urban Index (NDEUI)

208 In recent years, DMSP/OLS NTL was widely used to study urban sprawl, and several spectral
209 indices have been proposed. Zhang, et al. [46] proposed a new index VANUI combining MODIS
210 NDVI and DMSP/OLS NTL. Zhang, Li, Thau and Moore [28] proposed NDUI (Normalized Difference
211 Urban Index) combining ETM+ NDVI with normalized DMSP/OLS luminosity data to capture urban
212 spatial structures at a much finer scale. However, each annual NDVI composites was generated from
213 contiguous three-year ETM+ imageries, which will confuse changed land use types during the three
214 years, especially in the rapid development region. Furthermore, the thresholds of NDVI given by the
215 authors is nor suitable for all the cases. Cheng, et al. [47] constructed the BCI Assisted NTL Urban Index
216 (BANI) based on the correlations between BCI (Biophysical Composition Index) and normalized
217 DMSP/OLS NTL data. Here, the BCI was calculated using MODIS surface reflectance data, which not
218 only have several complex steps, including Tasseled Cap transformation but also only get the coarse
219 resolution BCI. Thus, in our study, we combine the EVI_{max} imagery mentioned in section 2.3.1 with the
220 30m resolution normalized DMSP/OLS NTL data to generate a new index, i.e. NDEUI (Normalized
221 Difference Enhanced Urban Index) (Eq.(2)).

222 $$NDEUI = (NTL - EVI)/(NTL + EVI) \quad (2)$$

223 Where NTL is the normalized DMSP-OLS stable nighttime lights data, and EVI is EVI_{max} imagery
224 generated from the all the 32-Day EVI Composites for one year.

225 *2.3 Classification with Random Forests*

226 According to the definition given by Schneider and Mertes [48], urban land is dominated by the
227 built environment with more than 50% coverage ratio within a landscape unit, which include all non-
228 vegetative, human-constructed elements (building, roads etc.). Thus, five land cover categories were

 doi:10.20944/preprints201810.0164.v1

classified from remote sensing imagery in this study, which are urban land, water bodies, agriculture/grassland, forest and barren land.

The annual classification was implemented utilizing optimal Landsat TOA Reflectance as the base scene and corresponding NDEUI. Due to the seasonal phenology of study area and cloud cover, a base scene with less cloud cover acquired from July to October was preferred. It should be noted that there are not DMSP/OLS NTL data before 1992 and after 2013. According to the Statistical Yearbook of Xuzhou City, there is no obvious urban land change during the two periods. Thus, the DMSP/OLS NTL data was replaced by the data of 1992 and 2013 in annual classification before 1992 and after 2013, respectively.

To reduce possible biases caused by training samples and get relatively classifiers, a hierarchical sampling scheme [5] was adopted in our study. Firstly, with the support of EVImax imagery in 2005 and Google Earth, training samples were collected on the cloud-based platform, i.e. Google Earth Engine. Consequently, they were loaded as initial training samples of a specific temporally adjacent year, and were rechecked to identify whether their types have been changed. We could reassign their types, move to corresponding positions or delete for the changed samples. Thus, we repeated the procedure and obtained all the training samples for all years.

Random Forests (RF) is an ensemble learning method for classification, regression and other tasks [49], which uses trees as base classifiers. It is also considered as a combination of many classifiers and conferred some special characteristics [50]. RF increases the diversity of the trees by making them grow from different training data subsets created through bootstrap aggregating (bagging), which is a technique used for training data creation by resampling the original dataset with replacement randomly [51]. Several research results have shown that RF classifier performs better than other well-known classifiers, because of its high efficiency, robustness to noise or outliers, high efficiency and lighter computation [50, 52, 53]. In addition, it has the capability of a bigger number of variables and quantitative measurement of variable contributions [5]. In theory, the RF classifier randomly selects a sample of the training set and a sample of variables many times to generate a large number of small classification trees. Then, all the small trees are aggregated to determine the final category by applying a majority vote rule [49].

Two parameters should be defined in RF classifier for generating a prediction model, which are the number of classification trees (k), and the number of prediction variables (m), used to split a RF node. In general, the generalization error always is convergent and over-training is not a problem due to the ''Strong Law of Large Numbers'' with increasing the number of trees [51]. As well as, in order to make each individual tree of the model to be less strong and reduce the correlation between trees, it is an effective approach to reduce the number of predictive variables (m). Thus, it is essential to optimize the parameters k and m to minimize the generalization error. In this study, based on the sensitivity experiment, we applied the RF classifier with 500 classification trees. The number of prediction variables (m) corresponds to the square root of the number of input variables [54]. The "Out-of-Bag" OOB accuracy was employed to assess the performance of classification for each year, which is an unbiased estimator of the classification OA accuracy and can be used to substitute the cross-validation [49]. Approximately 2/3 of the train data were used to train the classifier, while the remaining data to validate the training. After classification, the mode filter (3*3) was used for post-classification procedures like "salt-and-pepper" removal. Thus, the final LULC maps for 1985, 1995, 2005 and 2015 were generated (Figure 6).

Preprints (www.preprints.org) | NOT PEER-REVIEWED | Posted: 9 October 2018 doi:10.20944/preprints201810.0164.v1

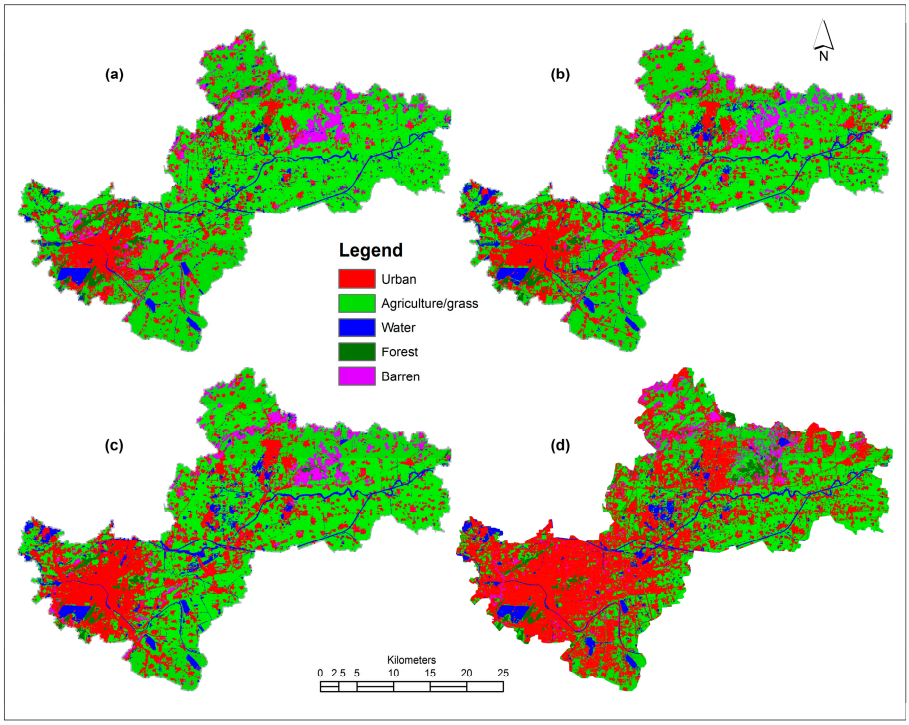

Figure 6. LULC maps of Xuzhou city for (a) 1985, (b) 1995, (c) 2005 and (d) 2015 derived from Landsat series imageries

2.4 Classification accuracy assessment

Accuracy assessment for individual classification is essential to correct and efficient analysis of LULC change. A total number of 100 pixels checked using Google Earth and knowledge of the study area for each class was collected on the basis of stratified random distribution method to conduct accuracy assessment of each classification. The error matrix, overall accuracy and Kappa coefficient were calculated for each classified land use maps and tabulated in Table 1 to Table 4, respectively. The overall accuracies ranged from 97.8% to 98.8%, with Kappa coefficients from 0.9725 to 0.985.

Table 1 Accuracy assessment for the 1985 LULC map produced from Landsat TM.

Classified data	Reference data						User's Accuracy [%]	Kappa Accuracy
	C1	C2	C3	C4	C5	Sum		
Urban land (C1)	96			3	1	100	96	0.95
Agriculture/grass land (C2)		100				100	100	1
Water bodies (C3)			100	3		103	97.09	0.9636
Forest (C4)				94		94	100	1
Barren land (C5)	4				99	103	96.12	0.9515
Sum	100	100	100	100	100	500		
Producer's Accuracy [%]	96	100	100	94	99			
Overall Accuracy [%]					97.8			
Kappa Coefficient					0.9725			

Preprints (www.preprints.org) | NOT PEER-REVIEWED | Posted: 9 October 2018 doi:10.20944/preprints201810.0164.v1

Table 2 Accuracy assessment for the 1995 LULC map produced from Landsat TM.

Classified data	Reference data						User's Accuracy [%]	Kappa Accuracy
	C1	C2	C3	C4	C5	Sum		
Urban land (C1)	95				2	97	97.94	0.9742
Agriculture/grass land (C2)		99				99	100	1
Water bodies (C3)		1	100	3		104	96.15	0.9519
Forest (C4)				97		97	100	1
Barren land (C5)	5				98	103	95.15	0.9393
Sum	100	100	100	100	100	500		
Producer's Accuracy [%]	95	99	100	97	98			
Overall Accuracy [%]						97.8		
Kappa Coefficient						0.9725		

Table 3 Accuracy assessment for the 2005 LULC map produced from Landsat TM.

Classified data	Reference data						User's Accuracy [%]	Kappa Accuracy
	C1	C2	C3	C4	C5	Sum		
Urban land (C1)	98	1			3	102	96.08	0.951
Agriculture/grass land (C2)		99				99	100	1
Water bodies (C3)			100			100	100	1
Forest (C4)				100		100	100	1
Barren land (C5)	2				97	99	97.98	0.9747
Sum	100	100	100	100	100	500		
Producer's Accuracy [%]	98	99	100	100	97			
Overall Accuracy [%]						98.8		
Kappa Coefficient						0.985		

Table 4 Accuracy assessment for the 2015 LULC map produced from Landsat OLI.

Classified data	Reference data						User's Accuracy [%]	Kappa Accuracy
	C1	C2	C3	C4	C5	Sum		
Urban land (C1)	100			2	5	107	93.46	0.9182
Agriculture/grass land (C2)		100			2	102	98.04	0.9755
Water bodies (C3)			100			100	100	1
Forest (C4)				98		98	100	1
Barren land (C5)					93	93	100	1
Sum	100	100	100	100	100	500		
Producer's Accuracy [%]	100	100	100	98	93			
Overall Accuracy [%]						98.2		
Kappa Coefficient						0.9775		

2.5 Land use change and landscape analysis

Land change analysis was carried out utilizing GIS-based spatial operations and landscape metrics derived from the LULC maps. In this paper, we focus on the land use changes during the period of 1985-1995, 1995-2005, 2005-2015 and 1985-2015, especially on the growth of urban land and its spatial change trend. Several qualitative and quantitative methods were employed to analyze the spatial landscape patterns changes of land use at different stages. Here, landscape patterns were evaluated utilizing

Preprints (www.preprints.org) | NOT PEER-REVIEWED | Posted: 9 October 2018 doi:10.20944/preprints201810.0164.v1

landscape metrics, which can be calculated on the three deferent levels, namely patch-level, class-level and landscape-level. In this study, class-level and landscape-level metrics were employed. Class-level metrics are used to qualify the characteristics of the same LULC type and return a unique value for each class in the landscape. On the other hand, landscape-level metrics return a unique value corresponding to the landscape mosaic as a whole [55]. In order to reduce the correlativity, landscape metrics selected in this study are tableted in Table 5 [56].

Table 5 List and descriptions of landscape metrics used in this study

Landscape metrics	Description	Level	Unit	Range
	General index			
PLAND (Percentage landscape)	To quantify the proportional abundance of each patch type in the landscape	Class	Percent	0 < PLAND ≦ 100
	Patch complexity			
PD (Patch density)	To quantify the density of patches for each class in the entire landscape	Landscape /Class	Number per 100 hectares	PD > 0
ED (Edge density)	To measure the perimeter for each class type per unit area	Landscape /Class	Meters per hectare	ED ≥ 0, without limit.
LSI (Landscape shape index)	To measure the shape index based on the perimeter-to-area ratio for each class type with regards to the entire landscape boundary	Landscape /Class	None	LSI ≥ 1, without limit
	Aggregation			
CONTAG	To measure what extent landscapes are aggregated or clumped as a percentage of the maximum possible	Landscape	Percent	0 < CONTAG ≦ 100
LPI (Largest Patch Index)	To quantify the percentage of total landscape area comprised by the largest patch	Landscape /Class	Percent	0 < LPI ≦ 100
AI (Aggregation Index)	To quantify the aggregation of different patch types and the spatial configuration characteristics of landscape components calculated from an adjacency matrix	Landscape /Class	Percent	0 ≦ AI ≦ 100
	Connectivity			
COHESION (Patch Cohesion Index)	To quantify the physical connectedness of the corresponding patch type	Landscape /Class	None	0 < COHESION < 100
	Diversity			
SHDI (Shannon's Diversity Index)	To measure relative patch diversity, or the proportional abundance of each patch type within the landscape	Landscape	Information	SHDI ≥ 0, without limit

Preprints (www.preprints.org) | NOT PEER-REVIEWED | Posted: 9 October 2018 doi:10.20944/preprints201810.0164.v1

Landscape metrics	Description	Level	Unit	Range
SIDI (Simpson's Diversity Index)	To measure the probability that any two pixels selected at random would be different patch types	Landscape	None	$0 \leqq SIDI < 1$

To visualize the spatiotemporal changes of landscape patterns and reveal their temporal and spatial characteristics during the urbanization, the LULC maps of the four years were divided into 900m × 900m grids using the gridsplitter plugin in QGIS, respectively. 1,424 subgrids were obtained in this study. The landscape metrics at landscape level for each subgrid were calculated using the Fragstats 4.2 to analysis spatiotemporal changes of landscape pattern.

3. Results and analysis

3.1 Change detection analysis

The changes detections were implemented for 1985-1995, 1995-2005, 2005-2015 and 1985-2015. Firstly, we calculated the net area changes by category between the different years based on the LULC maps (Figure 7). It is clear that urban land has significantly increased, while the agricultural land has been drastically reduced. It is also can be seen from the PLAND (Percentage of Landscape) of different land use in different years (Figure 8). During the period from 1985 to 1995, the urban area has increased by 6,082 ha that is more than 30.65%. In the next two decades, the urban area has increased by more than 10.54% and 68.78%, respectively (Figure 7, Figure 8, and Figure 9). It suggested a sharply ascending trend in the development of the urban area, especially from 2005 to 2015.

Figure 9 present the gains and losses in urban area during the different period. On the contrary, the agricultural land kept the peace of decrease and loosed 26,933 ha in the past 30 years. Overall, the urban area has significantly increased by about 143.75% in the past three decades, at the main expense of agricultural land in the study area. For the water bodies, there is an increase of 26.78%, which can be explained by the subsidence result from coal mining from 1985 to1995. In the next two decades, the government attached importance to the reclamation of subsidence, thus the water area has slightly decreased by 5.72% and 15.90%, respectively. In general, it can be noted that there were no significant changes in the area of water body. The forest increased the total number by 15.68%, while barren land decreased by 28.63%. The transition mainly occurred from agricultural land to urban land from 1985 to 2015. Figure 10 illustrate the transition from other land use types to urban land in different periods.

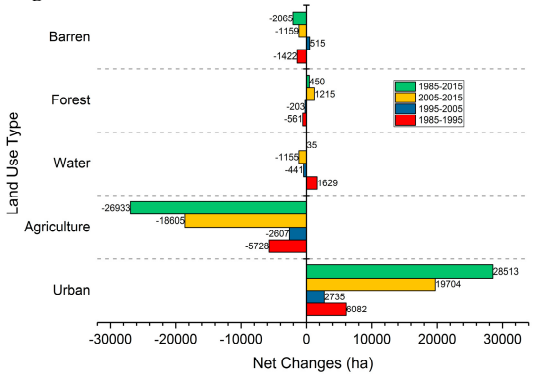

Figure 7. Net area changes by category between different years

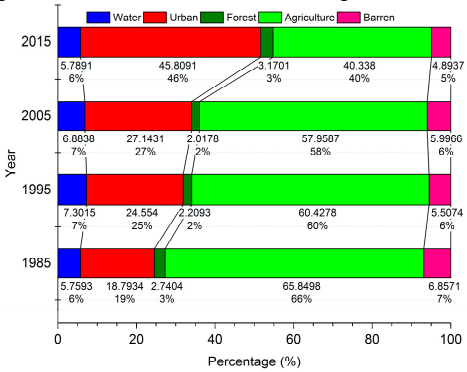

Figure 8. Proportion of area for each class type in the landscape

Preprints (www.preprints.org) | NOT PEER-REVIEWED | Posted: 9 October 2018 doi:10.20944/preprints201810.0164.v1

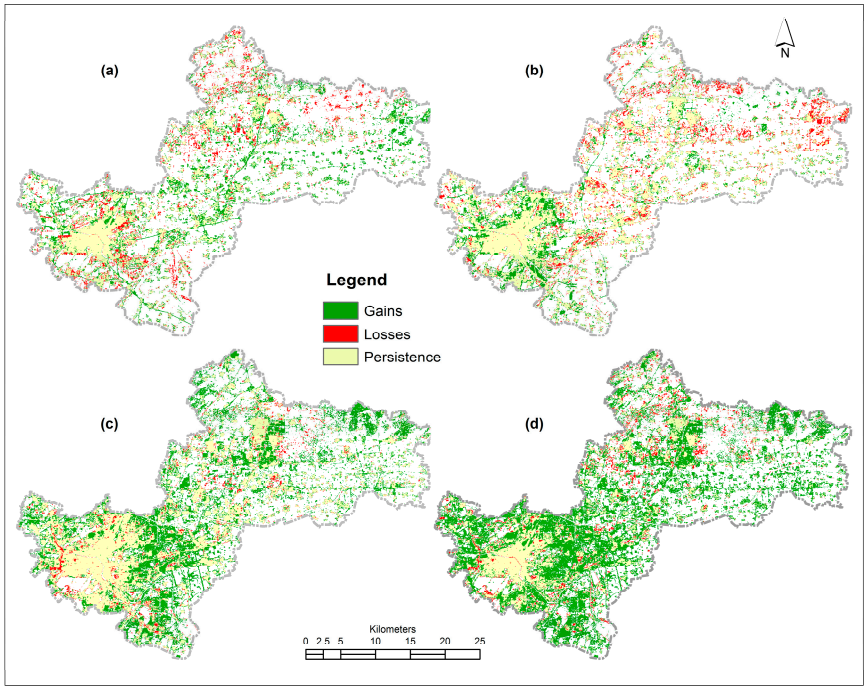

329

330 Figure 9. Maps presenting gains and losses in urban area during the period of (a) 1985-1995; (b) 1995-
331 2005; (c) 2005-2015; and (d) 1985-2015.

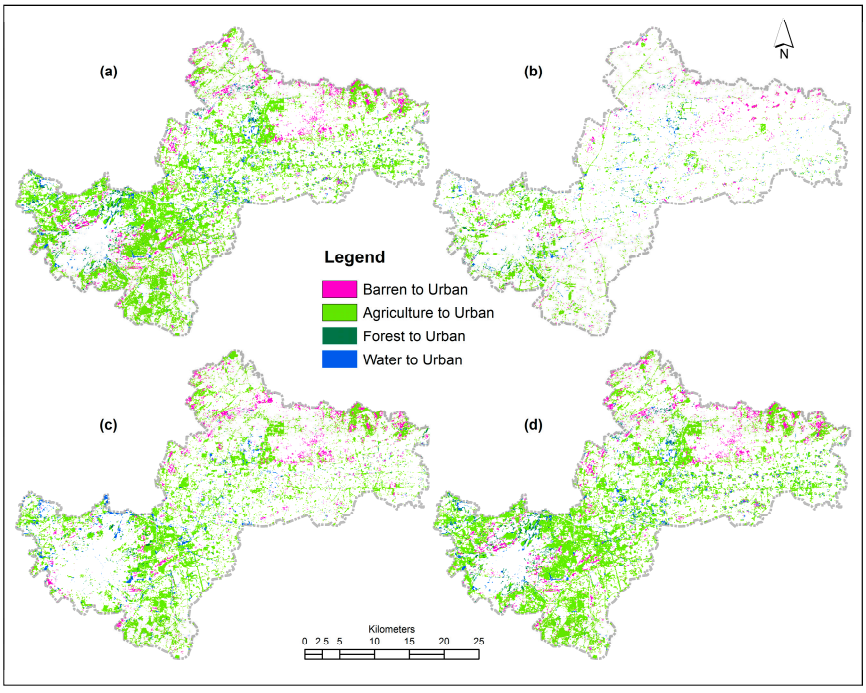

332

333 Figure 10. Maps of land use transition from other land use types to urban land during the period of (a)
334 1985-1995; (b) 1995-2005; (c) 2005-2015; and (d) 1985-2015.

335

Preprints (www.preprints.org) | NOT PEER-REVIEWED | Posted: 9 October 2018 doi:10.20944/preprints201810.0164.v1

3.2 Spatial trend of changes

In landscapes dominated by human intervention, patterns of change can be complex, and thus very difficult to decipher. Figure 11 shows the spatial sprawl of urban area in 1985, 1995, 2005 and 2015. To reveal the spatial trend of urbanization, we created the spatial trend maps of changes from other lands to urban land during the given periods adopting the 9th polynomial order, respectively (Figure 12).

As can be seen from the results, it is observed that continuous transition from other land use types into urban land has appeared dual-core development throughout urbanization process, which are main city region and Jiawang district, but with different development intensity in different periods. During 1985-1995, it is clear that there was a continuous increase in urban area between the two core regions from southwest to northeast (Figure 12 (a)). In the subsequent 10 years, however, the expansion in the urban area was mainly in all directions around the two core regions, especially in the main city region (Figure 12 (b)). During the period of 2005-2015, it is a remarkable fact that the growth in the southeastern part of the main city region was mainly due to the construction of new city region planned in 2004, which is also the location of municipal government (Figure 12 (c)). By the end of 2015, the total investment was up to about 70 billion yuan to construct the roads with the total length of about 110 km and 57 bridges, as well as the residential growth of more than 5 million square meters (Report on the Work of Xuzhou Municipal Government in 2016). As also can be seen in Figure 12(c), the high railway station available in 2011 gave the contribution to the growth of urban area. Overall, in the past three decades, the continuous increase in the urban area was mainly occurred between the new city region and the Jiawang district, mainly affected by construction of new city region, freeway and the high railway station (Figure 12 (d)). Compared with DEM (Figure 12(e)), terrain is also one of the factors, affecting the spatial trend of urban area changes. In the southwest and northeast of the study area, the topography undulated greatly and the degree of urbanization was lower than that of other areas.

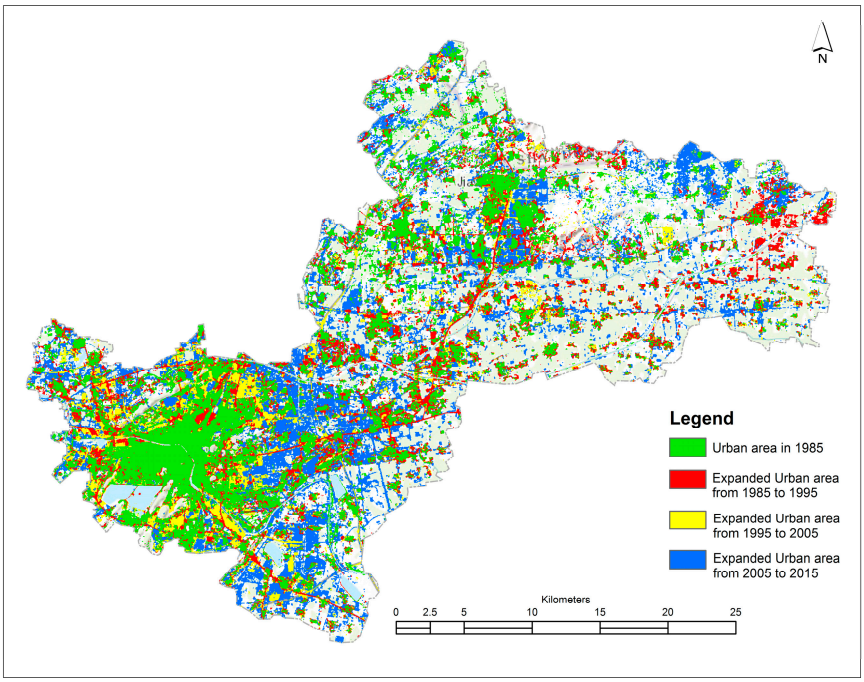

Figure 11. Spatial forms of urban sprawl in 1985, 1995, 2005 and 2015

Preprints (www.preprints.org) | NOT PEER-REVIEWED | Posted: 9 October 2018 doi:10.20944/preprints201810.0164.v1

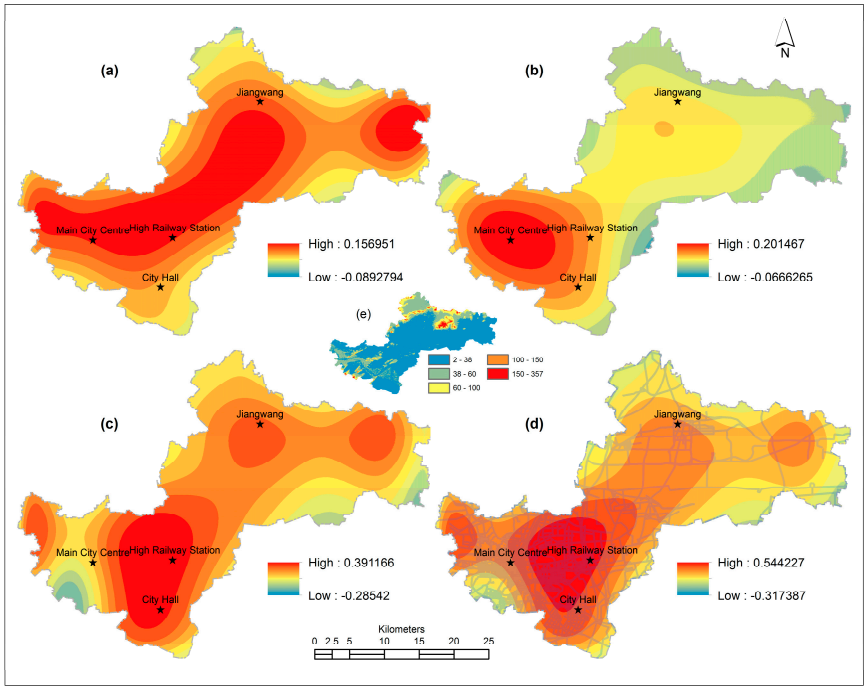

Figure 12. Spatial trend of urban growth during given periods: (a) from 1985-1995; (b) from 1995-2005; (c) from 2005-2015; (d) from 1985-2015, and (e) DEM of study area.

3.3 Changes analysis of landscape metrics

As shown in Figure 8 and Figure 10, the transition of land use types occurred mainly from agricultural land to urban land from 1985 to 2015. Thus, the changes and relationships measured based on different landscape metrics at the class level were analyzed between urban land and agricultural land. Here, the landscape metrics can be fit into four major categories to represent different aspects of the landscape pattern: Patch complexity (represented by PD, ED and LSI), aggregation (represented by LPI and AI), connectivity (represented by COHESION) and diversity (represented by SHDI and SIDI) (Table 5).

As can be seen from Figure 13, all the landscape metrics of urban land and agricultural land have undergone tremendous changes during the study period. In terms of PD, urban land use was on a downward trend while agricultural land use was continuously increasing (Figure 13 (a)). On the contrary, there was the consistent trend of changes in ED of agricultural land and urban land, reaching their lowest values in 2005, then dramatically increasing up to 48.853m/ha and 55.9287m/ha in 2015, respectively (Figure 13 (b)). Considering urban land, the date on LSI are interesting, the value decreased rapidly from 75.4532 in 1985 to 58.1453 in 2005, but then increasing again up to 68.1731 in 2015. The LSI of agricultural land appeared an overall increase from 41.6725 in 1985 to 64.2222 in 2015, except for a slight decrease in 2005 (Figure 13 (c)).

Figure 13 (d) illustrates that with significant decreasing in LPI of agricultural land, the LPI of urban Continued to increase, with an increase of more than 18.5%. Meanwhile, there was a gradual increase in AI of urban land, reaching 90.8229% in 2015. In term of agricultural land, however, it gradually dropped from 95.3672% in 1985 to 90.7922% in 2015 (Figure 13 (e)). Obviously, the aggregation of urban land gradually increased and surpassed that of agricultural land during the process of the past three-decade urbanization. With regard to COHESION, the values of agricultural land changed from 99.8371 to 99.0596, and urban land from 97.7713 to 99.6485 during the study period.

Preprints (www.preprints.org) | NOT PEER-REVIEWED | Posted: 9 October 2018 doi:10.20944/preprints201810.0164.v1

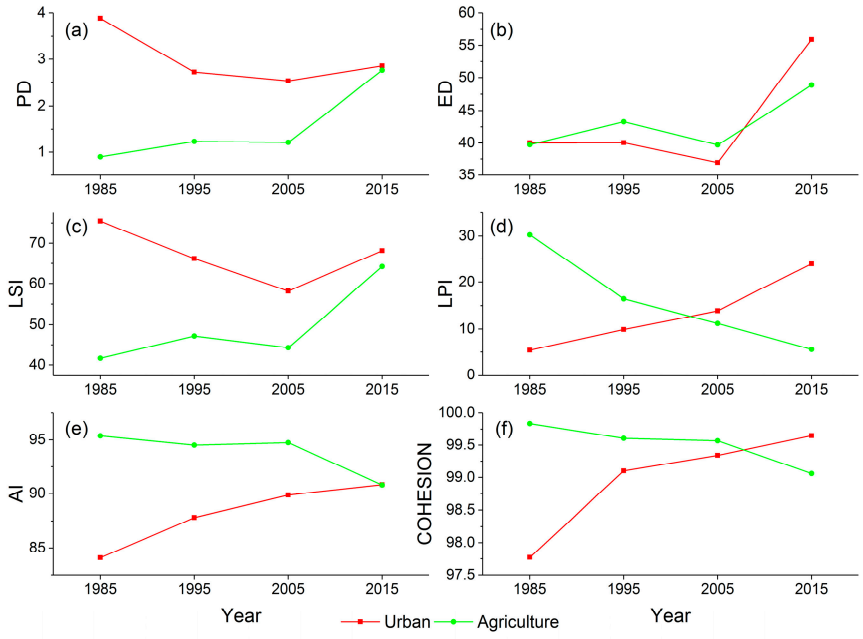

Figure 13. Line diagrams illustrating the changes and relationships of landscape metrics between the urban land and agriculture land at the class level.

Figure 14 shows the landscape-level metrics changes during the period of 1985-2015. The descriptions of landscape metrics used are tabulated in Table 5. As we can see from Figure 14(a to c), 2005 had the lowest patch complexity, increasing to their maximums in 2015. There is no doubt that the highest rates of change in the three metrics were observed in the period between 2005 and 2015. In terms of urbanization modes, this may indicate that infilling and edge-expansion modes were dominant in Xuzhou city before 2005, and then leapfrog mode. LPI declined from 30.2737% in 1985 to 13.9131% in2005, which may be the evidence that the agricultural land was dominant in 1985. However, it increased again to 23.9468% in 2015 (Figure 14 (d)). Combined with change detection discussed in 3.1, it could be concluded that the dominant land use type was shifted from agricultural land to urban land. It is clear from the Figure 14 that the CONTAG and AI metrics were considered to be inversely related to LSI. They tend to slightly fluctuate, but then dramatically decreased from the year 2005. This tendency affirmed that landscape pattern was vastly disaggregated and less contiguous pattern in 2015, mainly owing to continued increasing leapfrog urban land.

Figure 14 (g) shows the changes of the COHESION. The COHESION value decreased sharply, reaching its lowest value of 99.2116 in the year 1995. Thereafter it increased continuously in the late stage of urbanization.

Both SHDI and SIDI measure relative diversity. From 1985 to 2015 the two diversity metrics increased constantly (Figure 14 (h, i)), indicating an increasing heterogeneity in this landscape. This fact is already evident that agriculture became segmented into smaller patches as the continual increase in urban land.

Preprints (www.preprints.org) | NOT PEER-REVIEWED | Posted: 9 October 2018 doi:10.20944/preprints201810.0164.v1

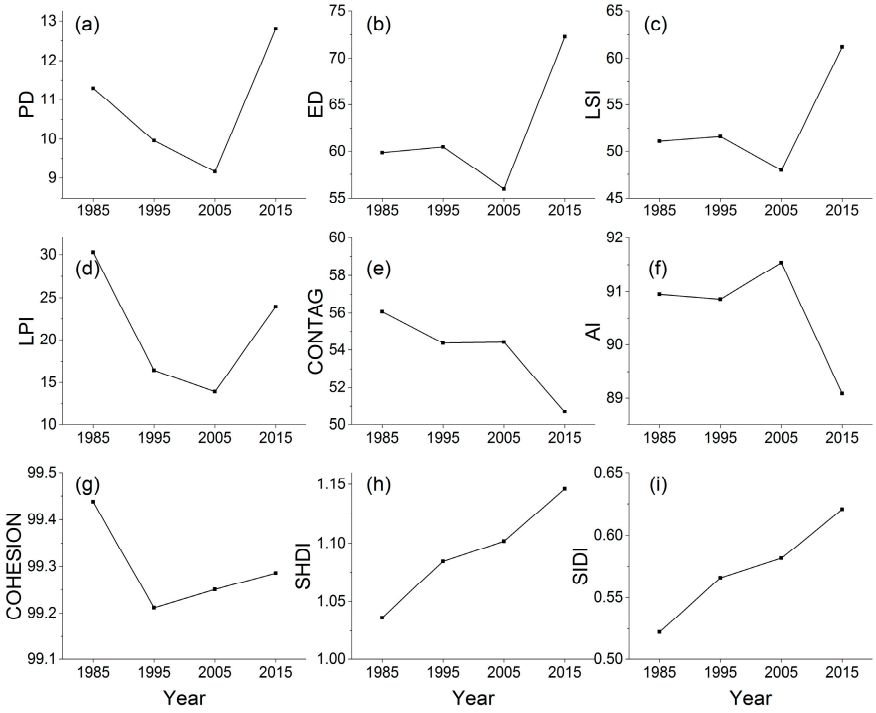

Figure 14. Line graph depicting the landscape-level metrics changes from 1985 to 2015

3.4 Spatiotemporal changes analysis of landscape pattern

At the landscape level, Landscape metrics calculated on the basis of subgrids well depict landscape pattern characteristics of each subgrid and contribute to revealing the spatiotemporal change of the study area. Furthermore, from the spatiotemporal changes of the landscape pattern, urban core, urban fringe, and rural area can be well discerned. Here, we mapped the spatial distribution of each landscape metric for different years utilizing the quantile grading method (Figure 15). It is clear that the landscape patterns have changed remarkably in the process of urbanization in Xuzhou City.

For the PD Landscape metric, urban core and rural areas are associated with lower values, which are mainly dominated by urban land and agricultural land, respectively, while urban fringe areas are opposite. From the perspective of spatiotemporal changes, the urban core area was expanding continuously, while the PD landscape metric in rural areas continued to increase, indicating that agricultural land was continuously transited into urban land and appear a tendency of fragmentation in the process of urbanization. AI, however, is opposite to PD, with higher values in urban core and rural areas and lower values in urban fringes. As can be seen from Figure 15, ED and PD have a similar spatiotemporal change tendency. During the process of urbanization, the values surrounding the urban core area had a slight decrease, which marked that the core area continued to expand. From the southeast to the northeast of the main urban region, however, the value has been obviously increasing, especially in 2015, mainly due to the construction of new city region and the high railway station resulting in a large amount of transition from agricultural land into urban land. As LPI is used to quantify the percentage of total landscape area comprised of the largest patch, it is a simple measure of dominance. For instance, LPI map (a) in Figure 15 gives prominence to old city region and distribution of agricultural land. With the fragmentation of agricultural land, LPI map (d) clearly highlight the urban core area. The COHESION maps reveal connectivity of the patches in the study area and represent the impact extent of urban expansion. Compared with COHESION map (a) in Figure 15, COHESION map (d) has obviously decreased in the southeast of the main city region, which just verifies the vigorous development of the

 doi:10.20944/preprints201810.0164.v1

new city region in recent years. Regarding SHDI, although there was a marked decrease in 2005, SHDI showed a significant increase trend, mainly due to the continuous expansion of the urban area and the promotion of a large number of municipal projects in recent years, including the construction of the freeways and the subways. Taking into account the evolution of urban, all landscape metrics used in this study were mutually corroborated in terms of spatiotemporal characteristics. The changes at landscape-level metrics in subgrids effectively reveal the spatiotemporal evolution process of urbanization during the study period.

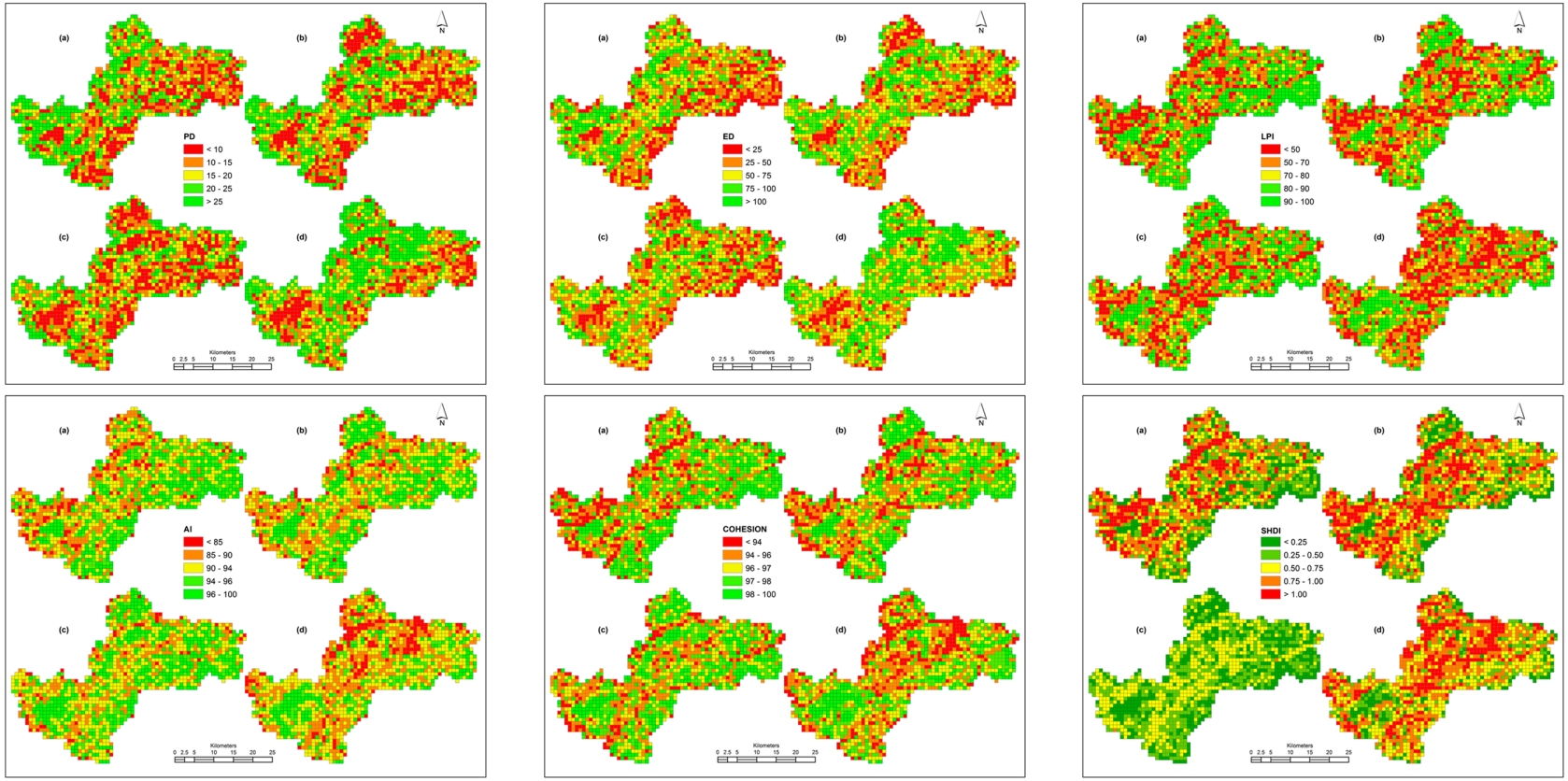

445 Figure 15. Spatiotemporal changes of landscape metrics: (a) 1985, (b) 1995, (c) 2005 and (d) 2015

doi:10.20944/preprints201810.0164.v1

Preprints (www.preprints.org) | NOT PEER-REVIEWED | Posted: 9 October 2018 doi:10.20944/preprints201810.0164.v1

4. Discussion

4.1 NDEUI as an effective index for improving the classification accuracy

An index NDEUI was proposed in this study, combined with annual maximum EVI and corresponding DMSP/OLS NTL, which effectively reduce confusion between urban areas and barren land, as well as fallows. The advantage owes to the fact that annual maximum EVI makes sure the agricultural lands have maximum EVI values obtained in growing seasons to decrease the impact from seasonal fallow lands. Furthermore, since barren lands, especially far away from urban area, are associated with extremely low value in NTL, DMSP/OLS NTL can effectively separate them from urban lands. It is necessary that 1-km resolution normalized NTL data downscale in the size of 30 m. Firstly, we generated annual maximum EVI from 32-Day EVI Composites for each year. Secondly, the NDEUI for each year was calculated. Afterwards, a new composite was generated combing with NTL, annual maximum EVI and Landsat raw bands, and used to obtain the land use classification by means of Random Forests classifier. In this study, all the procedures were implemented on a free cloud computing platform, namely Google Earth Engine. The GEE, based on its cloud-computing and storage capability, has archived a large number catalog of earth observation data and enabled researchers to work on the trillions of images online. It represents one of the most powerful tools up to now in remote sensing with its ability to analyze and classify remotely sensed data over different temporal scales. In this study, the GEE provided us an effective approach to obtain the land cover classifications by JavaScript.

4.2 Relationship of urbanization and changes dynamic of landscape pattern

Analysis the changes in landscape metrics contribute to demonstrate the urban growth modes in the different process of urbanization. Usually, there are three urban growth modes discussed in previous literature, i.e. infilling, edge-expansion and leapfrog mode [35, 57, 58]. In this study, several landscape metrics at class/landscape level depicted in detail in Section 3 were selected to characterize their spatiotemporal changes, generating a large quantity of information on landscape patterns. All the information could determine which urban growth mode was dominant, as well as indicate the degree affected by urbanization at different stage during the study period. The gradual changes in landscape metrics imply that the landscape was undergoing a major transformation from one dominant land cover to another resulting from urbanization. On the other hand, this dramatic land cover change caused by rapid urbanization has resulted in an essential change of landscape patterns. It could be clear that there are some inherent relationships between the process of urbanization and the changes in landscape metrics no matter at class or landscape level. Consequently, it is effective and feasible to study the urbanization utilizing landscape metric.

Considering the urban growth modes, the analysis based on the results are as follow. With a slight increase of infilling area, urban growth mainly occurred as leapfrog mode along both sides of the roads during the period of 1985-1995, resulting in a slightly decreased aggregation of the landscape. Subsequently, the urban growth mode shifted into edge-expansion. With the increasing of edge-expansion growth in urban area, the urban land has become more aggregated and compact at this stage, especially in the main city region, reflected by the decreasing PD, ED and LSI as well as the increasing AI. Since 2005, the process of urbanization was accelerated, and urban growth mainly appeared from the southeast to the northeast of the main city region, owing to the construction of new city region and other infrastructures. At this stage, the edge-expansion and leapfrog modes coexisted, causing different change degree of landscape metrics in different region. All the urbanization processes in different stages are reflected in spatiotemporal changes of landscape metrics.

 doi:10.20944/preprints201810.0164.v1

5. Conclusion

Urbanization is an irreversible process, and rapid urbanization has resulted in drastic changes in LULC and landscape patterns over the past three decades, particularly in the developing countries. Mapping and monitoring of LULC change, therefore, are crucial to generating information for policymakers and planners, as well as helping to understand the underlying socio-economic and biophysical processes in urban areas. Accordingly, a GIS&RS-based integrated approach was used to quantitatively characterize the land use/land cover pattern and dynamics of urban sprawl in Xuzhou city during the period of 1985–2015.

In this study, we integrated NTL with annual maximum EVI and proposed a new spectral index, namely NDEUI. NDEUI-assisted Random Forests algorithm was implemented to obtain the LULC maps in 1985, 1995, 2005 and 2015, respectively. The results indicate that the classification scheme proposed achieved higher accuracy, reducing confusion between urban areas and barren land, as well as fallows. The results show that Xuzhou city has experienced rapid urbanization over the past three decades. Urban areas have increased by 143.75%, covering approximate 2.44 times the urban area in 1985, resulting in a considerable decrease in agricultural land. Among the three decades, the highest growth in urban land is up to 68.78% from 2005 to 2015, averaging nearly 7% per year. As can be seen from the analysis of the urban growth spatial trend that the urban growth is proceeding in different directions during the different period. Overall, the urban growth has appeared dual-core development mode throughout the urbanization process. the process of urbanization in the north-east direction of the main city region, mostly appears growth of Industrial area in the first two decades, whereas, in the southeastern direction, the urban growth is mostly due to due to the construction of new city region planned in 2004 and the high railway station available in 2011, as well as accompanied the growth of residential area. It should be noted that the terrain and roads are also important factors affecting urbanization.

Statistical analysis may have a limited power to demonstrate the inherent relationship between LULC changes, accordingly the dynamic changes of landscape pattern affected by urbanization were studied. Six landscape metrics at the class level were calculated to reveal the dynamic changes of landscape pattern in urban land and agricultural land. The changes in selected landscape metrics indicate a lower aggregation and connectivity in agricultural land due to increasing dominance of urban land during the study period. On the other hand, nine landscape metrics were also calculated to indicate the landscape metrics changes at the landscape level. The landscape-level metrics changes suggest that there appeared an increasing spatial heterogeneity along with the process of rapid urbanization during the period of 1985-2015. Furthermore, to visualize the spatiotemporal changes of landscape patterns and reveal their temporal and spatial characteristics during the urbanization, we divided all the LULC maps into subgrids with the size of 900 m×900 m and calculated their landscape metrics at the landscape level. The findings suggest that different urbanization modes and intensity result in variously the spatiotemporal evolution of landscape patterns. In terms of urban growth mode, it can be concluded from the above analysis that the urban growth mainly appeared a leapfrog mode alone both sides of the roads during the period of 1985 to 1995, and then shifted into edge-expansion mode during the period from 1995 to 2005, whereas the edge-expansion and leapfrog modes coexisted for the period from 2005 to 2015, causing different change degree of landscape metrics in different region. Overall, the high valuable spatiotemporal information generated utilizing RS and GIS may give assistance to urban planners and policymakers to well understand urban dynamics and evaluate their spatiotemporal and environmental impacts at a local level for the sake of sustainable urban planning in the future.

Acknowledgments: We would like to express our respects and gratitude to the anonymous reviewers and editors for their professional comments and suggestions on improving the quality of this paper. This work was supported by the Visiting Research Scholar Program of the China Scholarship Council (Grant No. 201606425072), A Project Funded by the Priority Academic Program Development of Jiangsu Higher Education Institutions（PAPD）.

References

1. Zhang, J.; Li, P. J.; Wang, J. F., Urban Built-Up Area Extraction from Landsat TM/ETM plus Images Using Spectral Information and Multivariate Texture. *Remote Sensing* **2014,** 6, (8), 7339-7359.
2. Reynolds, R.; Liang, L.; Li, X. C.; Dennis, J., Monitoring Annual Urban Changes in a Rapidly Growing Portion of Northwest Arkansas with a 20-Year Landsat Record. *Remote Sensing* **2017,** 9, (1), 71.
3. Verhasselt, Y., Urbanization and Health in the Developing World. *Soc Sci Med* **1985,** 21, (5), 483-483.
4. Minshull, R., Urbanisation: Changing environments. *Geography* **1998,** 83, (360), 297-297.
5. Li, X.; Gong, P.; Liang, L., A 30-year (1984–2013) record of annual urban dynamics of Beijing City derived from Landsat data. *Remote Sensing of Environment* **2015,** 166, 78-90.
6. Li, X. C.; Liu, X. P.; Gong, P., Integrating ensemble-urban cellular automata model with an uncertainty map to improve the performance of a single model. *Int J Geogr Inf Sci* **2015,** 29, (5), 762-785.
7. Zhang, P.; Imhoff, M. L.; Bounoua, L.; Wolfe, R. E., Exploring the influence of impervious surface density and shape on urban heat islands in the northeast United States using MODIS and Landsat. *Can J Remote Sens* **2012,** 38, (4), 441-451.
8. Ceplova, N.; Kalusova, V.; Lososova, Z., Effects of settlement size, urban heat island and habitat type on urban plant biodiversity. *Landscape and Urban Planning* **2017,** 159, 15-22.
9. Schneider, A., Monitoring land cover change in urban and pen-urban areas using dense time stacks of Landsat satellite data and a data mining approach. *Remote Sensing of Environment* **2012,** 124, 689-704.
10. Lu, M.; Chen, J.; Tang, H. J.; Rao, Y. H.; Yang, P.; Wu, W. B., Land cover change detection by integrating object-based data blending model of Landsat and MODIS. *Remote Sensing of Environment* **2016,** 184, 374-386.
11. Coulter, L. L.; Stow, D. A.; Tsai, Y. H.; Ibanez, N.; Shih, H. C.; Kerr, A.; Benza, M.; Weeks, J. R.; Mensah, F., Classification and assessment of land cover and land use change in southern Ghana using dense stacks of Landsat 7 ETM + imagery. *Remote Sensing of Environment* **2016,** 184, 396-409.
12. Yang, Y. T.; Wong, L. N. Y.; Chen, C.; Chen, T., Using multitemporal Landsat imagery to monitor and model the influences of landscape pattern on urban expansion in a metropolitan region. *J Appl Remote Sens* **2014,** 8, (1), 083639.
13. Mihai, B.; Nistor, C.; Simion, G., Post-socialist urban growth of Bucharest, Romania – a change detection analysis on Landsat imagery (1984–2010). *Acta geographica Slovenica* **2015,** 55, (2), 223-234.
14. Schneider, A.; Friedl, M. A.; Potere, D., A new map of global urban extent from MODIS satellite data. *Environ Res Lett* **2009,** 4, (4).
15. Xian, G.; Homer, C.; Demitz, J.; Fry, J.; Hossain, N.; Wickham, J., Change of Impervious Surface Area Between 2001 and 2006 in the Conterminous United States. *Photogramm Eng Rem S* **2011,** 77, (8), 758-762.
16. Gong, P.; Wang, J.; Yu, L.; Zhao, Y. C.; Zhao, Y. Y.; Liang, L.; Niu, Z. G.; Huang, X. M.; Fu, H. H.; Liu, S.; Li, C. C.; Li, X. Y.; Fu, W.; Liu, C. X.; Xu, Y.; Wang, X. Y.; Cheng, Q.; Hu, L. Y.; Yao, W. B.; Zhang, H.; Zhu, P.; Zhao, Z. Y.; Zhang, H. Y.; Zheng, Y. M.; Ji, L. Y.; Zhang, Y. W.; Chen, H.; Yan, A.; Guo, J. H.; Yu, L.; Wang, L.; Liu, X. J.; Shi, T. T.; Zhu, M. H.; Chen, Y. L.; Yang, G. W.; Tang, P.; Xu, B.; Giri, C.; Clinton, N.; Zhu, Z. L.; Chen, J.; Chen, J., Finer resolution observation and monitoring of global land cover: first mapping results with Landsat TM and ETM+ data. *Int J Remote Sens* **2013,** 34, (7), 2607-2654.
17. Selkowitz, D. J.; Stehman, S. V., Thematic accuracy of the National Land Cover Database (NLCD) 2001 land cover for Alaska. *Remote Sensing of Environment* **2011,** 115, (6), 1401-1407.
18. Han, R.; Li, Z. L.; Ti, P.; Xu, Z., Experimental Evaluation of the Usability of Cartogram for Representation of GlobeLand30 Data. *Isprs Int J Geo-Inf* **2017,** 6, (6).
19. Liang, D.; Zuo, Y.; Huang, L. S.; Zhao, J. L.; Teng, L.; Yang, F., Evaluation of the Consistency of MODIS Land Cover Product (MCD12Q1) Based on Chinese 30 m GlobeLand30 Datasets: A Case Study in Anhui Province, China. *Isprs Int J Geo-Inf* **2015,** 4, (4), 2519-2541.
20. Li, G.; Lu, D.; Moran, E.; Hetrick, S., Mapping impervious surface area in the Brazilian Amazon using Landsat Imagery. *Gisci Remote Sens* **2013,** 50, (2), 172-183.
21. Lu, D. S.; Weng, Q. H., Spectral mixture analysis of the urban landscape in Indianapolis with landsat ETM plus imagery. *Photogramm Eng Rem S* **2004,** 70, (9), 1053-1062.
22. Boldt, M.; Thiele, A.; Schulz, K., Object-based Urban Change Detection Analyzing High Resolution Optical Satellite Images. *Earth Resources and Environmental Remote Sensing/Gis Applications Iii* **2012,** 8538.

23. Darwish, A.; Leukert, K.; Reinhardt, W., Urban land-cover classification: An object based perspective. *2nd Grss/Isprs Joint Workshop on Remote Sensing and Data Fusion over Urban Areas* **2003**, 278-282.
24. Forster, B. C., An Examination of Some Problems and Solutions in Monitoring Urban Areas from Satellite Platforms. *Int J Remote Sens* **1985,** 6, (1), 139-151.
25. Liu, C.; Shao, Z. F.; Chen, M.; Luo, H., MNDISI: a multi-source composition index for impervious surface area estimation at the individual city scale. *Remote Sens Lett* **2013,** 4, (8), 803-812.
26. Deng, C. B.; Wu, C. S., BCI: A biophysical composition index for remote sensing of urban environments. *Remote Sensing of Environment* **2012,** 127, 247-259.
27. As-Syakur, A. R.; Adnyana, I. W. S.; Arthana, I. W.; Nuarsa, I. W., Enhanced Built-Up and Bareness Index (EBBI) for Mapping Built-Up and Bare Land in an Urban Area. *Remote Sensing* **2012,** 4, (10), 2957-2970.
28. Zhang, Q. L.; Li, B.; Thau, D.; Moore, R., Building a Better Urban Picture: Combining Day and Night Remote Sensing Imagery. *Remote Sensing* **2015,** 7, (9), 11887-11913.
29. Li, S.; Chen, X., A new bare-soil index for rapid mapping developing areas using LANDSAT 8 data. *ISPRS - International Archives of the Photogrammetry, Remote Sensing and Spatial Information Sciences* **2014,** XL-4, 139-144.
30. Lu, D.; Mausel, P.; Brondizio, E.; Moran, E., Change detection techniques. *Int J Remote Sens* **2004,** 25, (12), 2365-2407.
31. Tewkesbury, A. P.; Comber, A. J.; Tate, N. J.; Lamb, A.; Fisher, P. F., A critical synthesis of remotely sensed optical image change detection techniques. *Remote Sensing of Environment* **2015,** 160, 1-14.
32. Jackson, T. J.; Chen, J. M.; Gong, P.; Liang, S.; Hassan, M. A. E. R. A. E. A., Integration of remote sensing (RS) and geographic information system (GIS) techniques for change detection of the land use and land cover (LULC) for soil management in the southern Port Said region, Egypt. *Land Surface Remote Sensing Ii* **2014,** 9260, 926032.
33. Son, N. T.; Chen, C. F.; Chen, C. R.; Chang, L. Y.; Thanh, B. X., Urban growth mapping from Landsat data using linear mixture model in Ho Chi Minh City, Vietnam. *J Appl Remote Sens* **2012,** 6, (1), 063543.
34. Villa, P., Mapping urban growth using Soil and Vegetation Index and Landsat data: The Milan (Italy) city area case study. *Landscape and Urban Planning* **2012,** 107, (3), 245-254.
35. Li, H.; Peng, J.; Yanxu, L.; Yi'na, H., Urbanization impact on landscape patterns in Beijing City, China: A spatial heterogeneity perspective. *Ecological Indicators* **2017,** 82, 50-60.
36. Chan, K. M.; Vu, T. T., A landscape ecological perspective of the impacts of urbanization on urban green spaces in the Klang Valley. *Applied Geography* **2017,** 85, 89-100.
37. Schwoertzig, E.; Poulin, N.; Hardion, L.; Trémolières, M., Plant ecological traits highlight the effects of landscape on riparian plant communities along an urban–rural gradient. *Ecological Indicators* **2016,** 61, 568-576.
38. Liu, T.; Yang, X. J., Monitoring land changes in an urban area using satellite imagery, GIS and landscape metrics. *Applied Geography* **2015,** 56, 42-54.
39. Chander, G.; Markham, B. L.; Helder, D. L., Summary of current radiometric calibration coefficients for Landsat MSS, TM, ETM+, and EO-1 ALI sensors. *Remote Sensing of Environment* **2009,** 113, (5), 893-903.
40. Huete, A.; Didan, K.; Miura, T.; Rodriguez, E. P.; Gao, X.; Ferreira, L. G., Overview of the radiometric and biophysical performance of the MODIS vegetation indices. *Remote Sensing of Environment* **2002,** 83, (1-2), 195-213.
41. Tan, M. H., Urban Growth and Rural Transition in China Based on DMSP/OLS Nighttime Light Data. *Sustainability-Basel* **2015,** 7, (7), 8768-8781.
42. Liu, Z. F.; He, C. Y.; Zhang, Q. F.; Huang, Q. X.; Yang, Y., Extracting the dynamics of urban expansion in China using DMSP-OLS nighttime light data from 1992 to 2008. *Landscape and Urban Planning* **2012,** 106, (1), 62-72.
43. Elvidge, C.; Hsu, F.-C.; Baugh, K.; Ghosh, T., National Trends in Satellite-Observed Lighting: 1992–2012. *In Global Urban Monitoring and Assessment Through Earth Observation* **2013**, 97-120.
44. Pandey, B.; Zhang, Q. L.; Seto, K. C., Comparative evaluation of relative calibration methods for DMSP/OLS nighttime lights. *Remote Sensing of Environment* **2017,** 195, 67-78.
45. Zhang, Q. L.; Pandey, B.; Seto, K. C., A Robust Method to Generate a Consistent Time Series From DMSP/OLS Nighttime Light Data. *Ieee Transactions on Geoscience and Remote Sensing* **2016,** 54, (10), 5821-5831.

46. Zhang, Q. L.; Schaaf, C.; Seto, K. C., The Vegetation Adjusted NTL Urban Index: A new approach to reduce saturation and increase variation in nighttime luminosity. *Remote Sensing of Environment* **2013,** 129, 32-41.
47. Cheng, Y.; Zhao, L. M.; Wan, W.; Li, L. L.; Yu, T.; Gu, X. F., Extracting urban areas in China using DMSP/OLS nighttime light data integrated with biophysical composition information. *J Geogr Sci* **2016,** 26, (3), 325-338.
48. Schneider, A.; Mertes, C. M., Expansion and growth in Chinese cities, 1978–2010. *Environ Res Lett* **2014,** 9, (2), 024008.
49. Breiman, L., Random forests. *Mach Learn* **2001,** 45, (1), 5-32.
50. Rodriguez-Galiano, V. F.; Ghimire, B.; Rogan, J.; Chica-Olmo, M.; Rigol-Sanchez, J. P., An assessment of the effectiveness of a random forest classifier for land-cover classification. *ISPRS Journal of Photogrammetry and Remote Sensing* **2012,** 67, 93-104.
51. Breiman, L., Bagging predictors. *Mach Learn* **1996,** 24, (2), 123-140.
52. Gislason, P. O.; Benediktsson, J. A.; Sveinsson, J. R., Random Forests for land cover classification. *Pattern Recogn Lett* **2006,** 27, (4), 294-300.
53. Chan, J. C.-W.; Paelinckx, D., Evaluation of Random Forest and Adaboost tree-based ensemble classification and spectral band selection for ecotope mapping using airborne hyperspectral imagery. *Remote Sensing of Environment* **2008,** 112, (6), 2999-3011.
54. Pelletier, C.; Valero, S.; Inglada, J.; Champion, N.; Dedieu, G., Assessing the robustness of Random Forests to map land cover with high resolution satellite image time series over large areas. *Remote Sensing of Environment* **2016,** 187, 156-168.
55. Cushman, S. A.; McGariyal, K.; Neel, M. C., Parsimony in landscape metrics: Strength, universality, and consistency. *Ecological Indicators* **2008,** 8, (5), 691-703.
56. McGarigal; K.; Cushman, S.; Ene., E. *FRAGSTATS v4: Spatial Pattern Analysis Program for Categorical and Continuous Maps. Computer software program produced by the authors at the University of Massachusetts, Amherst. Available at the following web site:* http://www.umass.edu/landeco/research/fragstats/fragstats.html, 2012.
57. Liu, X. P.; Li, X.; Chen, Y. M.; Tan, Z. Z.; Li, S. Y.; Ai, B., A new landscape index for quantifying urban expansion using multi-temporal remotely sensed data. *Landscape Ecol* **2010,** 25, (5), 671-682.
58. Sun, C.; Wu, Z. F.; Lv, Z. Q.; Yao, N.; Wei, J. B., Quantifying different types of urban growth and the change dynamic in Guangzhou using multi-temporal remote sensing data. *International Journal of Applied Earth Observation and Geoinformation* **2013,** 21, 409-417.